Automotive Research Center

A U.S. Army Center of Excellence for Modeling and Simulation of Ground Vehicles

Led by the University of Michigan

Control of a Lead-Acid Battery/Fuel Cell Hybrid Power System for a UGV: Experimental Report

Funded by:

U.S. Army Research Development and Engineering Command (RDECOM)

U.S. Army Tank Automotive Research, Development and Engineering Center (TARDEC)

In accordance with Cooperative Agreement W56HZV-14-2-0001

John A Broderick

Dawn M Tilbury

Ella M Atkins

December 2014

Control of a Lead-Acid Battery/Fuel Cell Hybrid Power System for a UGV: Experimental Report

John A Broderick, Dawn M Tilbury, and Ella M Atkins

December 19, 2014

1 Introduction

Future robotic vehicles including both small unmanned ground vehicles (UGVs) and full-scale vehicles will carry multiple sources of power, including batteries, fuel cells, combustion engines, ultracapacitors, and/or solar cells, to allow for long-endurance operation. Fuel-based power sources have a higher specific energy than batteries, the reason most current automobiles are gasoline-powered. Batteries have other advantages, such as low noise profile, easy replacement, and direct energy conversion. Solar energy harvesting exploits natural resources to increase total energy reserves. Long-term missions, especially for autonomous robots that can operate indefinitely without human contact, will require power systems operated together at maximum system efficiency. Ongoing research in the Automotive Research Center (ARC) looks at integration of multiple power sources for ground robots together to increase energy efficiency and mission duration.

As part of the proposed work for ARC project 1.13: Reconfigurable Control for Energy and Thermal Management in Unmanned Vehicles, hardware tests were conducted at TARDEC in the Ground Systems Power and Energy Laboratory (GSPEL) to validate the models and methodology that had been developed for optimization of multiple power sources. For these tests, the power system consists of an AMI 200 W solid oxide fuel cell and a TALON lead-acid battery pack; this fuel cell was designed to power small ground robots and is easily mountable on a TALON. The goals of these tests were twofold: verify that average power provides sufficient information for optimization purposes and demonstrate effectiveness of optimization compared to baseline control scheme. Details of the optimization are presented in [3].

This report is organized as follows. Related work and an overview of the optimization method is presented in Section 2. Section 3 details the hardware system used. Section 4 details the modeling of the TALON battery pack for use in the optimization. Battery Performance under averaged and variable power demands is summarized in Section 5 and validation of the optimization routine is presented in Section 6. Conclusions and Lessons Learned are presented in Section 7.

2 Background and Scope of Experiments

2.1 Related work

While current UGVs are almost universally battery powered, new research is looking at replacing or augmenting the battery with a fuel cell. Wilhelm et al. present a UGV powered exclusively by a fuel cell [11]. Their robot was quite small, using a 10 W fuel cell, and served as a proof of concept. Joh et al. present a humanoid robot powered by a fuel cell and a battery in parallel [6]. The authors demonstrate the use of their robot, including the use of the battery to supplement the

fuel cell when the power demand exceeds the capacity of the fuel cell. However, the fuel cell is able to vary the power output and there is no discussion of charging the battery when power demands are low.

Hybrid power sources are a major area of interest in the automotive industry [5]. Most of the work is based on a combustion engine/battery hybrid. However, there are some initial investigations into a fuel cell/battery hybrid automobile [10]. Ceraolo et al. presents a general approach to hybrid power architectures for automobiles [4]. For cars, due to the fact that the engine produces mechanical power and the battery produces electrical power, one of the key design decisions is between a parallel, series, or more complex power connection. Optimization for these different configurations have been studied (see [1, 7], for example).

More recently, Murphey et al. presented a power management scheme for a vehicle with multiple power sources [8]. Each individual source can be turned on or off, in addition to any throttling allowed by the device. Using a machine learning algorithm, the controller can decide at each time step which power sources are the best to use. While this algorithm has the same purpose as our algorithm, there are several key differences. First, their model assumes that the power sources can be turned on and off instantaneously and, second, their optimization looks over a short time horizon and not over an entire mission.

2.2 Optimization Method

To increase the mission life of a small ground robot, we have proposed a hybrid power modeling framework to control the power system by selecting which power sources to use [3]. Due to the long transients in startup/shutdown of the fuel cell under consideration, we consider power system use over an entire mission. To solve this problem, we simplify the models to a form where the optimization of the entire mission can take place in a short amount of time. This involves only using the average power of the mission and averaging the dynamics of the different power systems to meet the required simplifications.

Previously, we had considered a power system consisting of the 200 W fuel cell and a BB2590 Li-ion battery pack [3]. We used an existing model of the battery to run the optimization and schedule fuel cell on/off times for a long-duration mission. Figure 1 compares the simplified model to the full nonlinear model for the optimal schedule of fuel cell operation. For this power system simulation, the simplifications do not introduce significant errors.

To compare the effectiveness of our optimization algorithm, we also propose a simple controller based on the battery state of charge (SOC). The fuel cell is turned on (off) when the SOC reaches a low (high) threshold. These thresholds are chosen conservatively so that the battery is never depleted before the fuel cell is turned on while there is a 200 W load on the system and the entire power output from the fuel cell can be used to charge the battery. Figure 2 shows the total energy usage over a mission using the optimization and this conservative control scheme. The optimization scheme uses about 10% less power over the course of the entire mission.

2.3 Scope of Work

Having developed and compared this optimization in simulation, the next step is to validate the models and assumptions used in a hardware setting. There are two main goals in these tests: confirm that battery performance using an averaged power demand is sufficiently similar to performance under variable power demands and validate the optimization model against the real system.

While the simulation results are based on the BB2590 battery pack, due to incompatibilities between the fuel cell and the battery pack, a TALON lead-acid battery pack is used for the tests.

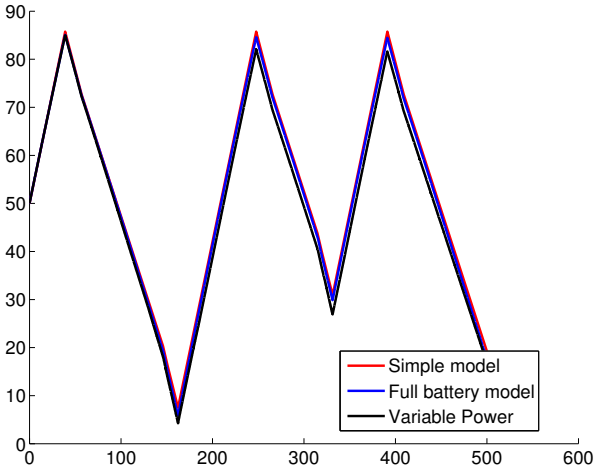

Figure 1: Comparing optimization model with full system model

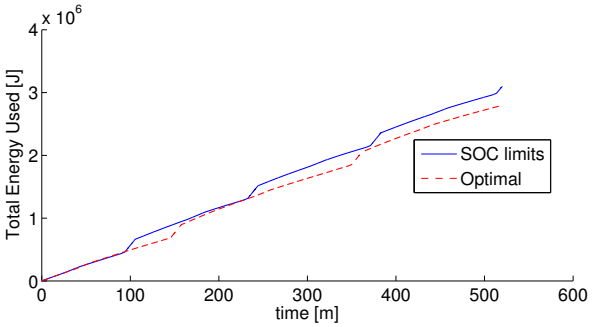

Figure 2: Comparing energy usage between baseline controller and optimal scheduling

This requires that a model of the lead-acid battery be developed and integrated into the optimization routine in place of the BB2590 model. This model, along with all the experience and data acquired from setting up and running the experience, are beneficial for future TARDEC projects looking at powering the TALON with the fuel cell.

3 Hardware Setup

This section details the experimental setup for the fuel cell/battery hybrid power system. Using the fuel cell in parallel with the TALON battery kit and the data logger designed by the GSPEL Fuel Cell Lab, the battery and fuel cell currents and system voltages can be measured. The load bank can be controlled to follow any given power profile. This setup allows for the load bank to emulate a robot power demand and to measure the power produced by the fuel cell and battery during system operation.

3.1 Ultra Electronics AMI Fuel Cell

The Ultra Electronics AMI Fuel Cell under test is a 200 W propane solid oxide fuel cell. The fuel cell can be turned off and on by the small button on top of the fuel cell or by connecting to an external laptop. The connection is made through the small headphone jack on the top of the fuel cell and a USB-serial converter connected to the laptop. AMI has provided a LabVIEW executable to control the device.

The propane canisters are connected to the fuel cell through a propane filter. The tanks are positioned on a scale to measure the current amount of fuel. The propane

(a) Fuel Cell (b) Propane Setup

Figure 3: AMI fuel cell with fuel tanks

tanks plus connectors weigh about 5.6 lbs when full and about 3.5 lbs when empty, though these values are dependent on the arrangement of the system. The tanks and scale were on the bottom shelf of the cart and the filter and fuel cell on the top of the cart.

3.2 TALON Battery

The fuel cell is designed to work with the TALON lead acid battery pack. This pack consists of 3 motorcycle batteries in series to produce the required voltage. The battery is B.B. Battery HR9-12. Each battery has a capacity of 8 Ah and 288 Wh and, combined in series, produce 36 V.

3.3 BK Precision Load Bank

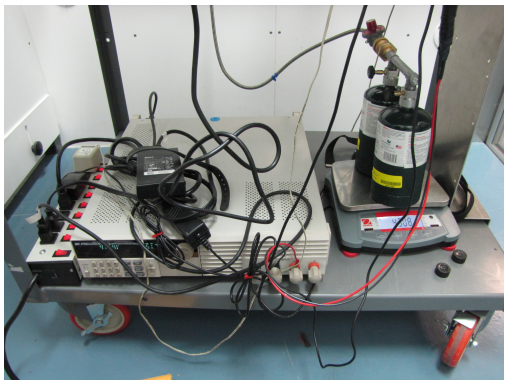

Figure 4: Load Bank

The load bank used is a BK Precision 8510. The load bank can be controlled manually or through a serial interface. LabVIEW modules are provided to initiate the serial communication and control system operation. Only two modes of operation were used: constant current (for logger calibration) and constant power. There are also constant voltage and and constant resistance modes. For each mode of operation, the constant parameter (i.e. current for constant current) can be specified. The load bank requires a ttl input for serial communication. This setup used a ttl/USB converter to connect to the external laptop. The power input connects to the input terminals on the front of the device.

3.4 Data Logger

The data logger for this system was designed by the GSPEL fuel cell lab. This logger consists of 2 battery connectors (on the same side), a fuel cell connector, and a load connector. The logger has an 8 pin header that outputs data voltages. With pin 1 closest to the load connector, the pins are as follows:

Pin	Description
1	Battery Current Sensor Output
2	Fuel Cell Current Sensor Output
3	Stepped-down System Voltage
4	External Input
5	External Input enabled
6	Unconnected
7	Unconnected
8	Ground

The logger does not record these data fields. Instead, we connected the relevant pins to an NI-9205 Data Acquisition Unit housed in a NI-cDAQ. Using LabVIEW, the sampled data from the logger is read from the DAQ and scaled to the actual values. To calibrate the different fields, the following procedures were used.

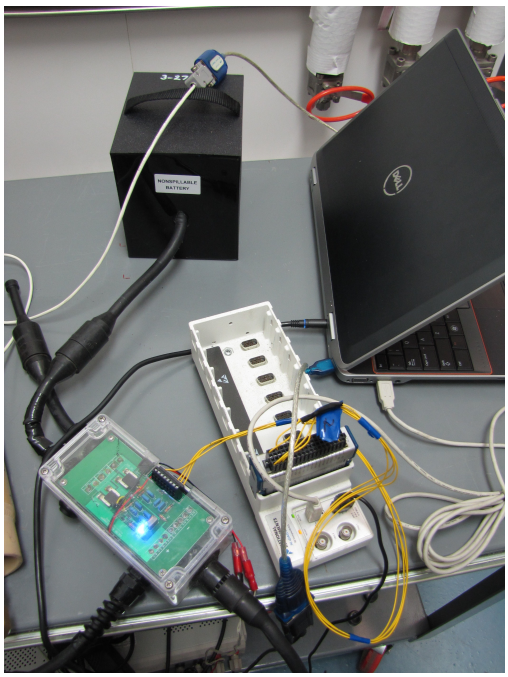

Figure 5: Battery and Logger

Voltage The system voltage is stepped-down through a resistor network to about 10% of the real value. By comparing the voltage readings at the load bank for a 0 W command, the system voltage output is 10% of the actual voltage.

Current Sensor The data logger has 2 ACS756 current sensors, measuring the battery and fuel cell current individually. The current sensor output voltage scales linearly with the measured current. The 2 important calibrations are the bias and scale. The bias is the output voltage when zero current is measured. Nominally, the bias is half the VCC applied to the sensor (about 5 V in this setup). The bias can be easily measured by setting the load to 0 W and measuring the output voltage. The scale is how much the voltage changes per amp of measured current (in the sensor documentation, the term sensitivity gives how much the voltage changes per amp). Nominally, the scale is 25 A/V. To calibrate the scale, after setting the bias, set the load bank to draw a constant current. With the known current the scale can be calculated.

The logger was modified to have an external power supply instead of a 9V battery. The battery can be reconnected by removing the top cover and loosening the board. On the backside, the external power supply wires can be disconnected and the battery carriage reconnected.

3.5 LabVIEW

The external laptop interfaces with the different components using LabVIEW. The basic outline of the program is to initialize communication, initialize power command data from file, record data outputs and send power commands for the duration of the test, then close communications. There are different loops for communication with each device and these loops end when the final time is reached, the stop button is pushed, or there is an error in any communication stream. While the communication loops occur asynchronously, all recorded data is marked with a synchronized measurement time.

A new output folder based on the current time is created and 6 files are made: system parameter (mainly current sensor calibration values), power command, load bank measurement, fuel weight measurements, battery state of charge measurements and data logger measurements. Each is in csv file format, with a row for each time step. The power command has the following columns: time, command. The fuel weight file has the following columns: time and weight. The SOC file has the following measurements: time, measured SOC (based on integrating current), and estimated SOC (values are meaningless and never tuned). The load bank file has the following columns: time, voltage, current, power. The data logger file has the following columns: voltage, battery current, fuel cell current. This data is logged at a constant sample rate that is set on the main panel. In these tests, we mostly used 100 Hz.

The power command input file is formatted the same as the output file and the command is linearly interpolated based on the current time and the closest two command points. The communication blocks for the load bank include a 200 ms delay, so the power command is only updated every 200 ms.

4 Battery Modeling

Due to the change in battery types between the simulation and the hardware tests, one of the first tasks was to determine a battery model that could be used in the optimization. This was done by tuning a lead-acid battery model used by ARC project 1.10 to the batteries used in our setup [9].

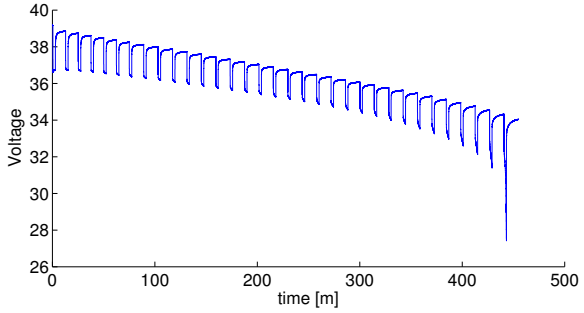

(a) Voltage over time, showing rapid discharges followed by voltage relaxation

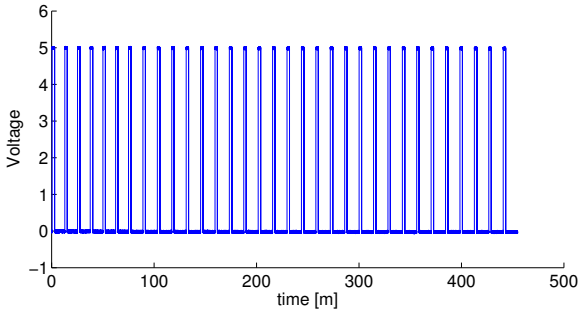

(b) Repetitive current profile

Figure 6: Example pulse-relaxation test

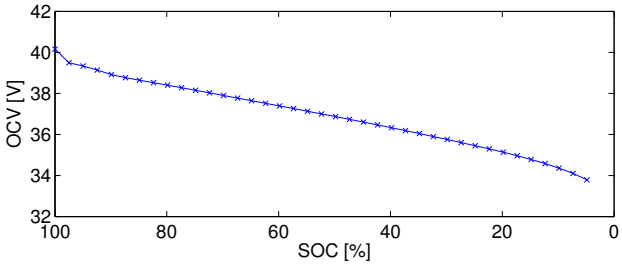

Figure 7: OCV as a function of SOC

There are two main steps to finding the battery model: finding the open circuit voltage (OCV) as a function of state of charge and fitting the resistance/capacitance values to match the battery performance.

4.1 Pulse-Relaxation tests

To find the OCV, we use a pulse-relaxation test. The battery was initially charged and then a constant current was drawn from the battery for a set time. The SOC is computed by integrating the current draw. The battery is allowed to rest for a period of time while the voltage rebounds. The OCV is measured once the voltage has stabilized and the process is repeated. Figure 6 shows the voltage and current profiles for one such test. From this test, the resulting OCV data is shown in Figure 7.

Table 1: OVC values for different SOC

SOC (%)	100.0	97.5	95.0	92.4	89.9	87.4	84.9	82.4	79.9	77.4	74.8	72.4	69.8
OCV (V)	40.2	39.5	39.3	39.1	38.9	38.8	38.6	38.5	38.4	38.3	38.2	38.0	37.9
SOC (%)	67.3	64.8	62.3	59.8	57.3	54.8	52.3	49.8	47.3	44.8	42.3	39.8	37.3
OCV (V)	37.8	37.6	37.5	37.4	37.3	37.1	37.0	36.9	36.7	36.6	36.5	36.3	36.2
SOC (%)	34.8	32.3	29.8	27.3	24.8	22.3	19.8	17.3	14.8	12.3	9.8	7.3	4.9
OCV (V)	36.0	35.9	35.8	35.6	35.5	35.3	35.1	35.0	34.8	34.6	34.4	34.1	33.8

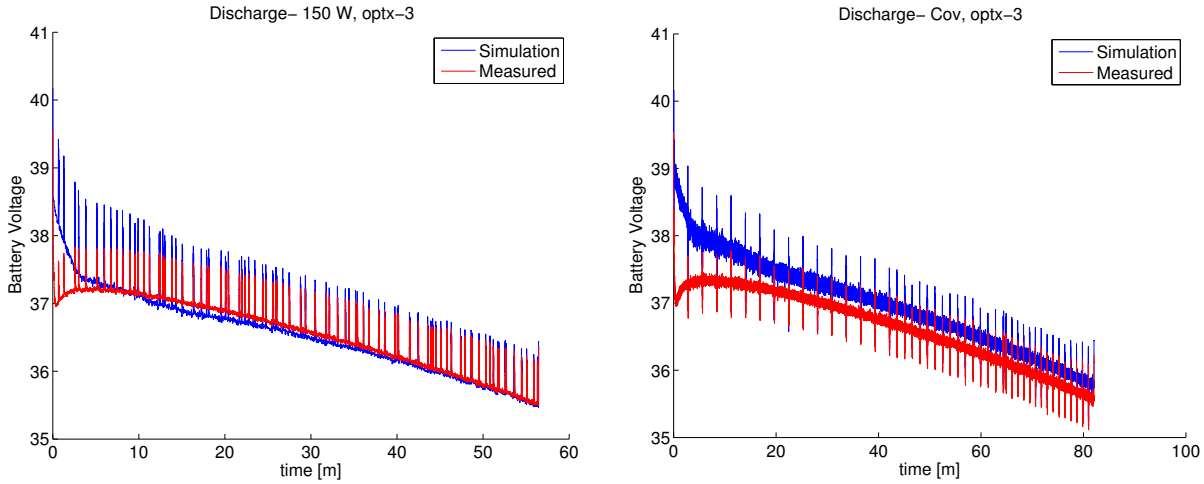

Figure 8: Comparing battery model and measured voltage for two different power demands

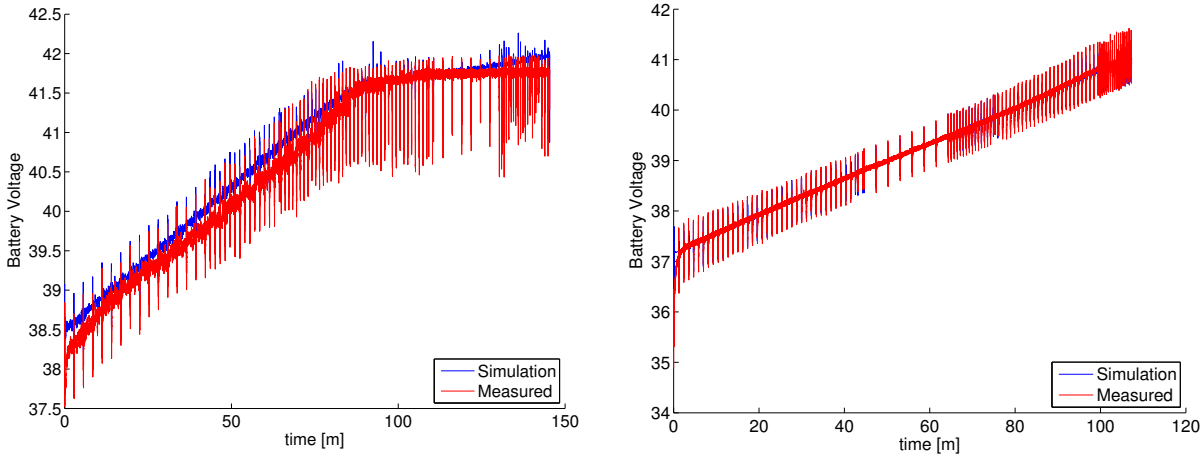

Figure 9: Comparing battery model and measured voltage while charging

4.2 Battery model

The OCV-R-RC battery model from [9] presumes an OCV source in series with a resistor and an RC circuit. With the OCV known, the other parameters of the model must be found. The primary resistance R is parameterized by soc s as $R = as^2 + bs + c$. The RC circuit parameters are assumed to be constant over all SOC values. The quality of our curve fit was determined by the squared difference between the simulated voltage and the measured voltage. Different parameters were found for charging and discharging.

A series of experiments were conducted to tune the battery parameters, including pulse-relax and discharge/charge tests. The parameters varied slightly between the different tests. Figures 8 and 9 compare the battery simulation and the experimental measurements for the discharge and charge profiles respectively. Model parameters were chosen by averaging the best fit parameters for the different test cases. In the discharge tests, there is an interesting rebound in the measured voltage at the beginning of the test, which is not accounted for in the simulation model. This rebound is possibly due to battery heating. It is unclear if this is a common phenomenon in lead-acid batteries; however, it is very common in our tests. The tail portion of the simulation matches

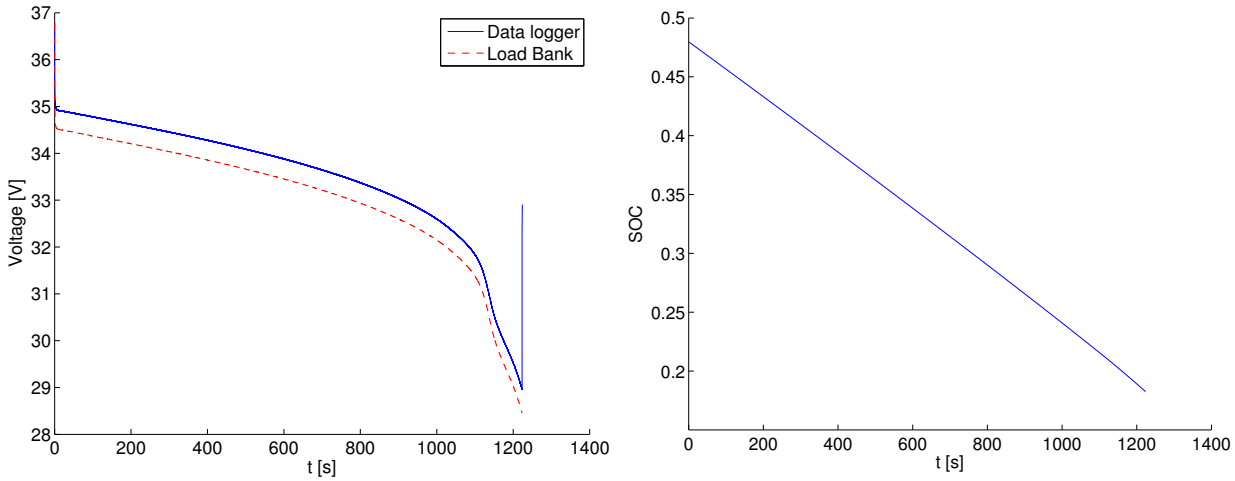

(a) Voltage

(b) State of charge

Figure 10: Battery reaches cutoff voltage before depletion

the experimental results quite well. For the charging case, the model matches the acquired data closely.

4.3 Other Battery Considerations

For power system optimization, the other key components of the model are the low SOC cutoff and the charging characteristics. The SOC thresholds for the baseline control scheme depend on these battery parameters.

In one test shown in Figure 10, the battery voltage reached the lower voltage cutoff of 29 V at about 18% state of charge. The voltage at the load bank is slightly lower then the data logger due to resistance in the wires between the logger and the load bank. The power demand for this test was a constant 230 W. As such, we define the low limit on the state of charge as 18% for our model. For optimization, we also introduce a safety margin to prevent the battery voltage from getting too close to the lower SOC limit.

To determine charging characteristics of the combined fuel cell/battery system, the fuel cell was started with the battery at a lower state of charge and the battery was allowed to charge until full. As the battery charges, the system voltage increases until the voltage converters in the fuel cell reach an upper limit. At this point the charging current decreases as the battery state of charge (and OCV) continues to increase. From experimental data, we pull out the charging curve, shown in Figure 11. The curve is fairly piecewise-linear; at low SOC, the charging rate is constant based on the maximum current available for the power output of the fuel cell above the mission demand. In this setup, this current matches the maximum charging current from the battery specifications. Once the battery reaches an SOC threshold, the charging current decreases at a linear rate.

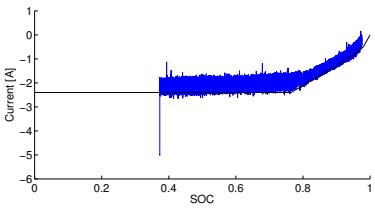

Figure 11: Current Charging Profile for Lead-Acid Battery

4.4 Variation Between Batteries

Each individual battery will have different performance. A total of four different batteries were used during the summer tests. Two of the batteries were older and had been used quite a bit with the TALON. As such, their operating characteristics were quite degraded. The other two batteries, which were the ones used for all the tests described above, were new and had nearly identical behavior. As shown in Figure 12, the new battery lasts longer than either of the old batteries, particularly old battery 2. While old battery 1 lasted close to the same time as the new battery, the difference was great enough to affect the battery model used in the optimization. This also shows how much the system model might change over the life a component; a model that fits well for a new device would need to be adjusted as the device ages.

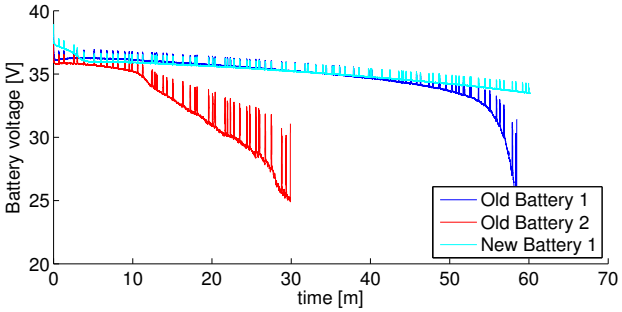

Figure 12: Comparing Battery Performance

5 Battery Performance Under Different Power Demands

The first tests look at comparing battery performance under averaged and time varying power demands. One of the main assumptions in our optimization algorithm is that the averaged power demand is a valid approximation of time varying power demand. The simulation models suggested this approximation was valid; the purpose of these tests was to verify that assumption in hardware.

Each test consists of operating the power system (battery and fuel cell) to meet a known power demand time history. The basic power demand for these tests is given by the area coverage trajectory [3]. To prevent battery charging currents from exceeding the maximum charging current, a 30 W peripheral power demand is added. This power demand is consistent with constant power demands for this type of robot [2]. The power demand, obtained through simulation, is smooth; to add more realism, we also introduced different power loads with more variation in the power demand over time. Figure 13 shows the different power demand profiles. The variability is a random gaussian sample with the variance taken from tests described in [2]. The "Low Bandwidth Variability" power demand has variability added every 3 seconds and the "High Bandwidth Variability" power demand has variability added every 0.2 seconds.

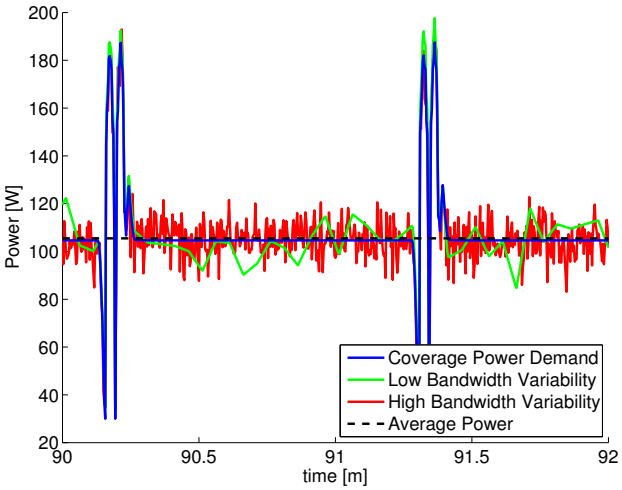

Figure 13: Portion of power demands used in tests

Four sets of tests were run. Each set was run on the same battery for repeatability. The first set was completed with more variability in the initial battery state of charge, prompting the subsequent sets of tests. The second set of tests were run on a different battery and gave conflicting results, prompting the third set on the same battery. The fourth set of tests were run on battery used in

Table 2: Amp-hour during charge and discharge

(a) Second set

	Cov. Path	Low Band.	High Band.	Avgerage
Discharge	6.02	5.9276	6.88	6.83
Charge	3.65	3.87	4.31	4.88

(b) Third set

	Cov. Path	Low Band.	High Band.	Avgerage
Discharge	6.75	6.83	6.37	6.89
Charge	4.86	4.85	4.43	4.81

the first tests to compare battery performance.

5.1 Test Procedure

The tests were run using the following procedure. First, the battery was discharged to about 40% SOC (36.35 V open circuit). The battery was allowed to rest to make sure the desired voltage was achieved. Next, the fuel cell was turned on and allowed to start up. During this time, the power system was under no load and the battery output current was recorded. When the fuel cell started producing power, the test was started and the load bank began to draw power according to the desired power profile for the test. Due to the variability of the fuel cell startup time, the battery was at slightly different levels of charge when the tests began. The battery was allowed to charge until power input to battery averaged around 20 W. The fuel cell was shut off and the test continued until the battery reached the low cut off voltage.

5.2 Test results

The tests were divided into charging and discharging portions due to the fact that the fuel cell is shut off at different times. Without this division, the discharge portions of the test could not be readily compared. In each case, we compared the battery voltage and current and the time required to charge/discharge the battery.

Figure 14 shows the results from the first set of tests. In these tests, the starting state of charge of the battery was not as uniform at the beginning of the test. Because of this variability, the start times of the "High Bandwidth Variability" and "Low Bandwidth Variability" cases are shifted. This shift was determined manually to counteract the differences in starting state of the battery. After completing this test, a more thorough test procedure was devised to eliminate the need for this manual adjustment.

In these tests, there is close agreement between the voltage and current over time during charge and discharge phases. The total time for discharging the battery is also roughly equal between the different tests. Compared to the "Average Power" case, the "Coverage Path" and "Low Bandwidth Variability" tests take 2.7% and 0.5% longer respectively to discharge and the "High Bandwidth Variability" takes 0.8% less time to discharge.

Figure 15 shows the voltage and current during charging for the second and third test sets. In the second set, there is some large differences between the current draws. The "Average Power" and "High Bandwidth Variability" tests have current draws that decrease linearly at the tail end of the charging cycle while the "Coverage Path" and "Low Bandwidth Variability" have closer to an exponential curve. In the third set, the current decreases linearly in all of the tests.

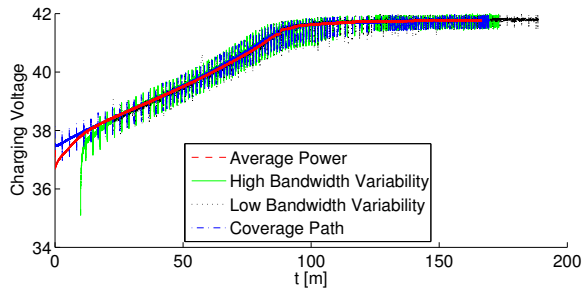

(a) Voltage while charging

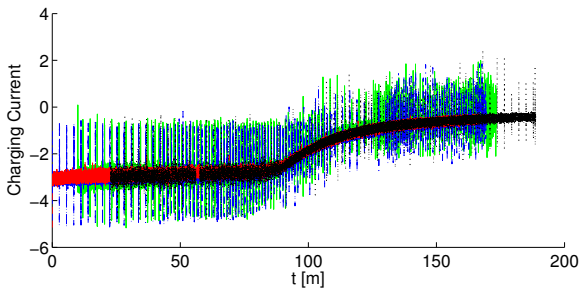

(b) Current while charging

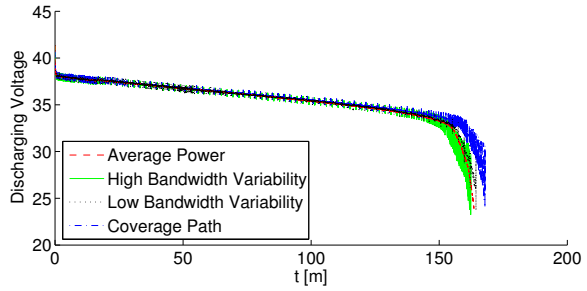

(c) Voltage while discharging

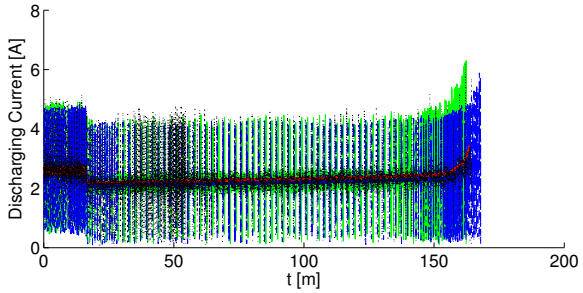

(d) Current while discharging

Figure 14: Comparison plots for set 1

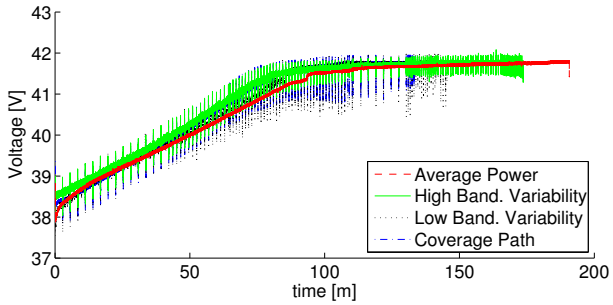

(a) Second Set- Voltage

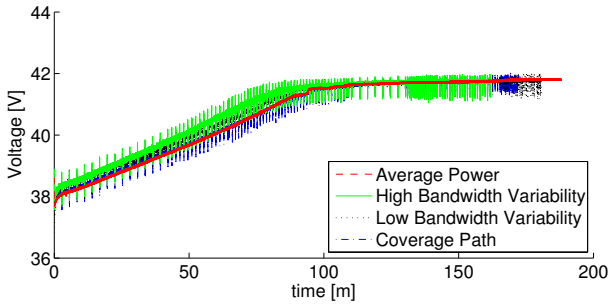

(b) Third Set- Voltage

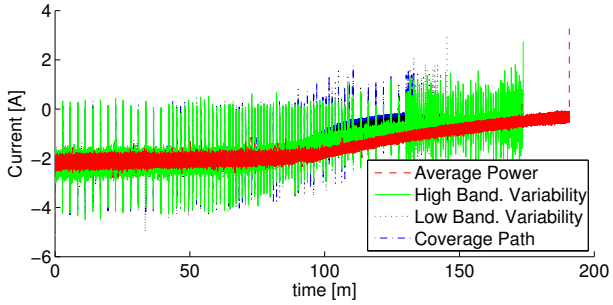

(c) Second Set- Current

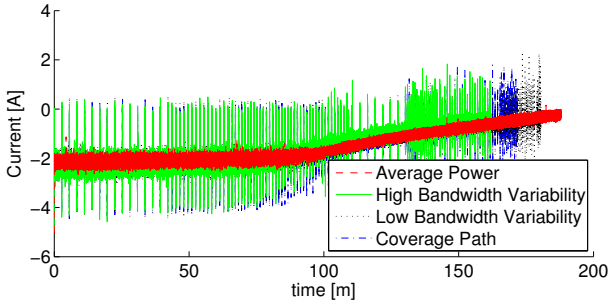

(d) Third Set- Current

Figure 15: Battery performance while charging

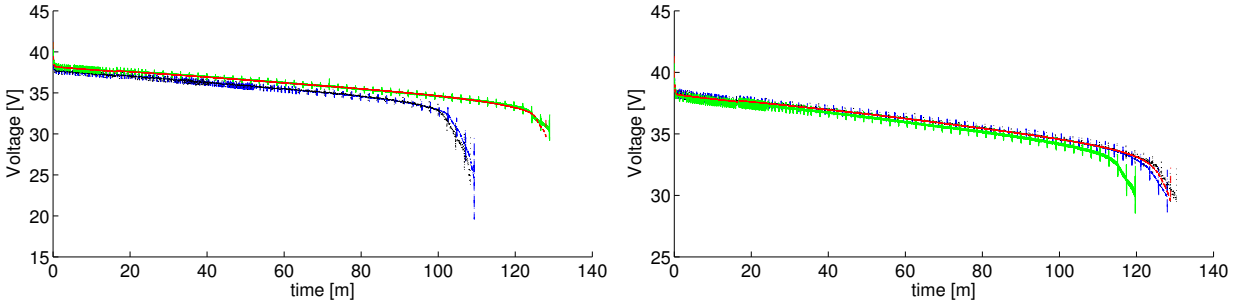

(a) Second Set (b) Third Set

Figure 16: Battery voltage while discharging

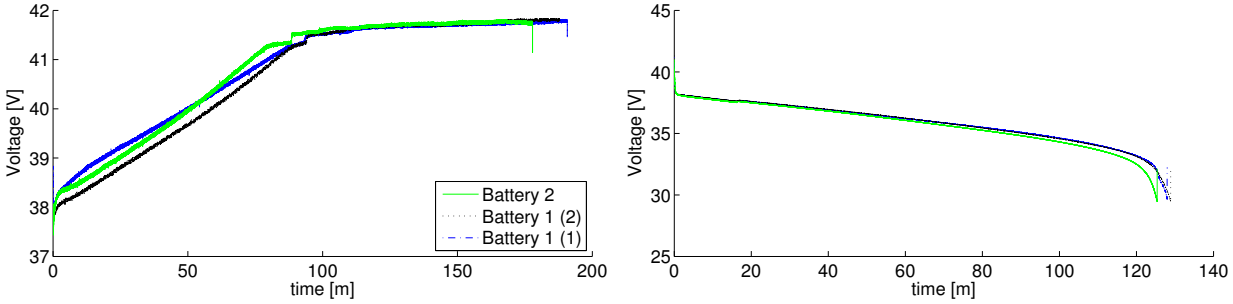

(a) Coverage path (b) Average power demand

Figure 17: Comparing different batteries in same test

Figure 16 shows the data for the discharge portion of the same sets of tests. The second set has significant variation, both in time to depletion and in the Amp-hour values in Table 2. It is unknown why this is. In contrast, the third set has close agreement between the different tests, with the exception of the high-bandwidth variability test. In particular, the battery is depleted faster in the high-bandwidth variability than the other tests. The discharge time is 7.1% less than the "Average Power" test and uses 7.5% less current before full discharge, but has 7.9% less current during the charging phase, accounting for the discrepancy in discharge time. The difference in the high-bandwidth test is clearly visible. The "Coverage Path" power demand discharges the battery in 0.66% less time and the "Low Bandwidth Variability" discharges the battery in 1.2% more time than the average power case.

The forth set of tests were run to compare the two different batteries in use. Figure 17 compares the "Average Power" tests from the second, third, and forth sets of tests. There is close agreement between the different batteries. We cannot compare with the first set of tests because the power demand was 30 W lower in the first set.

6 Validation of Optimization

The first step of validating the optimization was to update the simulation battery model to include the new lead-acid battery. For this, we used the model described in the Section 4. The most important part is to determine the battery charging characteristics. Shown in Figure 18 is the breakdown between the low charge and mostly charged states. This plot is very similar to the breakdown for the BB2590 pack, though the drop off in charging is more linear than the BB2590.

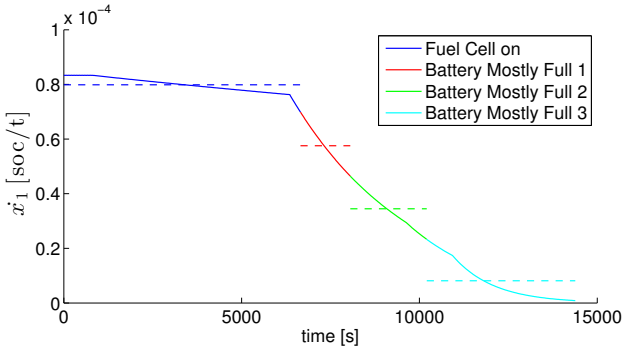

Figure 18: Battery charging dynamics broken up into discrete states

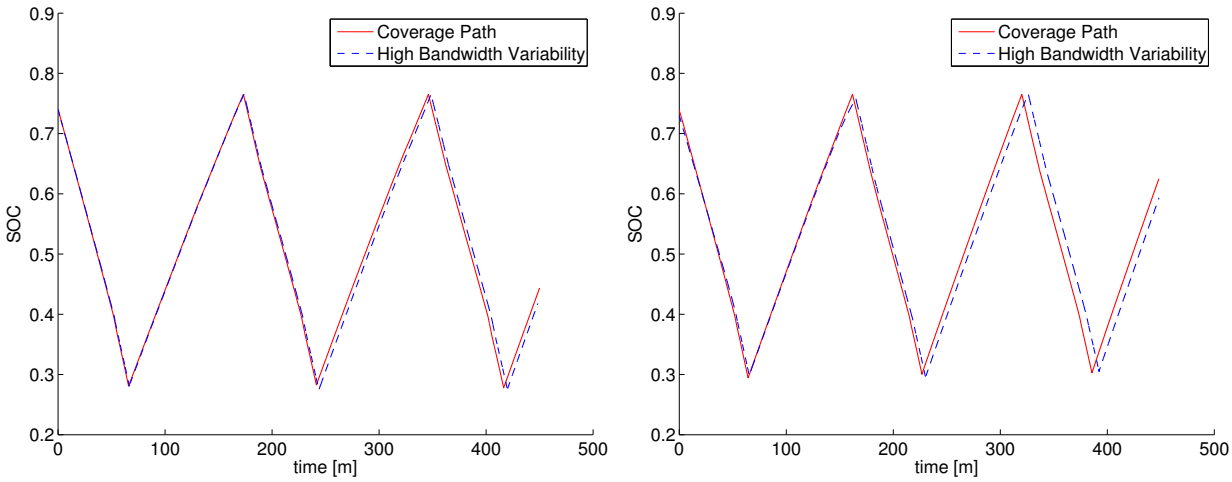

(a) First set

(b) Second set

Figure 19: Comparing battery SOC for different power demands using the SOC-limit controller

Per the battery spec sheet, the battery has a maximum charging current of 2.4 Amps. While the variable current does exceed this limit, a 30 W peripheral load was added to the system to prevent overcharging the battery on average. While we are using two different battery packs for these tests, the battery model simulated the battery performance of both batteries sufficiently well that the optimization is valid for both batteries.

The fuel cell model also had to be slightly changed based on observations from working with the fuel cell. First, the fuel draws about 6 W while off, presumably to power control electronics on board. Also, the real power output for the fuel cell varies slightly from the published 200 W. One of the fuel cells tested averaged 193 W and the other fuel cell averaged 198 W. The average startup and shutdown times were also updated based on the recorded data. The variation between the fuel cells, both power output and the startup/shutdown time, is an important note that must be accounted for in the optimization model.

In the SOC-limit case, we have two different sets of data, depending on which fuel cell was used for the test. The first fuel cell failed after completing the first set of tests and the tests were rerun with the new fuel cell to compare performance between the different fuel cells. The first set (Figure 19a) shows close agreement between the two trajectories, while there is more disagreement in the second set (Figure 19b). This difference is partially due to differences in initial conditions and

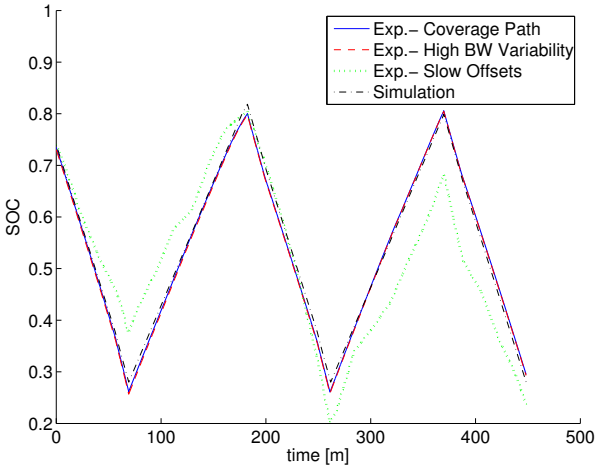

Figure 20: Comparing Actual battery SOC with optimization model

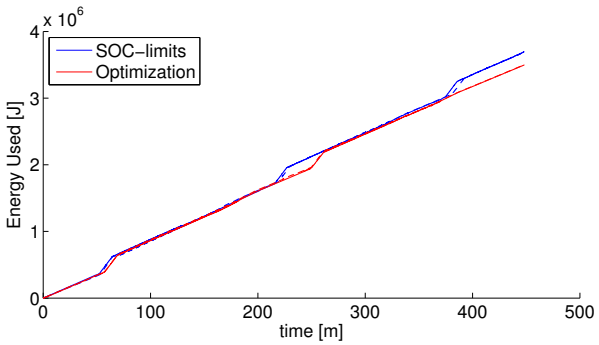

Figure 21: Energy usage for the SOC-limits and optimization tests (Solid line- cov. power demand, dashed line- high band. variability power demand

a experimental error resulting in a slightly delayed (about 30 s) fuel cell restart. Due to different fuel cell outputs, the data between fuel cells cannot be compared, however.

Figure 20 shows similar close agreement for the same tests using the optimization controller. There is close agreement between the optimization model and the experimental tests. This supports our use of the approximation in the optimization routine.

Figure 21 compares the energy used over the course of the mission. To compute energy usage, we use the weight of fuel consumed, scaled by the energy density of propane and the thermal efficiency of the fuel cell, and the change in energy storage in the battery. The energy remaining in the battery for a given SOC is calculated using the battery model. Using the unscaled propane energy would change the scale of the plot would be changed dramatically and hide what the optimization is doing. This plot agrees closely with Figure 2 from simulation. This plot was determined using actual fuel consumption and battery SOC, while the simulation plots were calculated by integrating the power outputs from the battery and the fuel cell.

The optimization controller was run with an additional power demand. This power demand had a very low bandwidth variability in addition to the high bandwidth variability. In this case, a power offset was calculated for each 700 second portion of the trajectory. The average power demand for this trajectory was the same as the average power for the baseline trajectory. This is similar to a robot that runs on constant terrain for a period, then on a different surface with slightly different characteristics. Due to the large differences over time, the battery SOC is expected to deviate from the baseline test. This test was an experiment to see how far the averaging assumption can be taken. As shown in Figure 20, there is a large discrepancy over time due to the unexpected power demands. Additionally, the battery charging limits are encountered in the first charging cycle, leading to a lower SOC at the end of the mission. This test shows the limits of the power demand assumption used in the optimization. If the moving power average differs greatly from the overall average, the battery can reach unsafe or inefficient operating conditions that the optimization routine cannot predict. In this case, the power strategy would need to be adapted during the mission based on measured power usage. This adaptation is left for future work.

7 Conclusions and Lessons Learned

7.1 Conclusions

The results from these experiments confirm the assumptions that underpin the optimization routine that was developed to maximize energy efficiency for a hybrid robot power system. In particular, we showed that average and time varying power demands result in similar battery life and performance. The optimization routine is also able to conserve energy over the course of a mission and extend ground robot performance.

These experiments also pointed out the sensitivity of the optimization algorithms on the power system components. When there is any variability in the components, whether startup times on the same fuel cell or power output in different fuel cells, the optimization model can produce incorrect results. As such, a safety buffer must be added to the optimization to prevent the robot from running out of energy over the course of the mission. Future research needs to address this deficiency in the model.

7.2 Lessons Learned

Only two fuel cells were used during the tests this summer. One unit, labeled SYS0020R02N0022, was used for the majority of the tests before it began to fail during startup. The second unit, labeled SYS0020R02N0017, was used exclusively for the long duration tests (both SOC-limit control and optimization).

The first major issue that occurred with the fuel cell was that it would occasionally turn off during use. This was not a normal shutdown; it would be operating then immediately turn silent and the LabVIEW program would lose connection with the device. This occurred two or three times with the first fuel cell and once with the second fuel cell. After restarting the LabVIEW program, the fuel cell would be listed in the off state. The only anomalous reading that I could tell was that the temperature sensors would show impossible data. One sensor would read 0 and the other would read 650 exactly. After a short time, the numbers would switch back to real values (in the 600-700 range). Whenever this occurred, the fuel cell would be started up momentarily, then shutdown before ignition began, allowing the fuel cell to enter the cool down state and return the device to a safe condition for restarting. The file "Data 140714 113814.txt" records the data from the fuel cell after the device was restarted. Unfortunately, the data logging was never turned on when the fuel cell shut down.

The other major issue with the fuel cell was that the first device started to fail on startup. It only occurred when the fuel cell was started soon after being shutdown. Sometimes the fuel cell would pop as normal, but would take several minutes to get to that point, at which point it would immediately fail.

For the first fuel cell, the startup time average about 820 seconds. One interesting point, which might be related to the failure described above, is that the fuel cell would take longer to start up on when it had recently been operating, taking closer to 900 seconds. The second fuel cell had a faster startup time, averaging about 740 seconds, though there were fewer startups to base the data on. For this fuel cell, repeat startups took less time (about 40 seconds less).

The shutdown time is very consistent at 1000-1010 seconds for both fuel cells.

References

[1] Stefano Barsali, C. Miulli, and A. Possenti. A control strategy to minimize fuel consumption of series hybrid electric vehicles. *Energy Conversion, IEEE Transactions on*, 19(1):187–195, 2004.

[2] John A. Broderick, Dawn M. Tilbury, and Ella M. Atkins. Characterizing energy usage of a commercially available ground robot: Method and results. *Journal of Field Robotics*, 31(3):441–454, 2014.

[3] John A Broderick, Dawn M Tilbury, and Ella M Atkins. Modeling and scheduling of multiple power sources for a ground robot. In *Proceedings of the ASME DSCC 2014*, 2014.

[4] M. Ceraolo, A. Di Donato, and G. Franceschi. A general approach to energy optimization of hybrid electric vehicles. *Vehicular Technology, IEEE Transactions on*, 57(3):1433–1441, 2008.

[5] C.C. Chan. The state of the art of electric, hybrid, and fuel cell vehicles. *Proceedings of the IEEE*, 95(4):704–718, 2007.

[6] Han-Ik Joh, Tae Jung Ha, Sang Youp Hwang, Jong-Ho Kim, Seung-Hoon Chae, Jae Hyung Cho, Joghee Prabhuram, Soo-Kil Kim, Tae-Hoon Lim, Baek-Kyu Cho, Jun-Ho Oh, Sang Heup Moon, and Heung Yong Ha. A direct methanol fuel cell system to power a humanoid robot. *Journal of Power Sources*, 195(1):293 – 298, 2010.

[7] Chan-Chiao Lin, Huei Peng, J.W. Grizzle, and Jun-Mo Kang. Power management strategy for a parallel hybrid electric truck. *Control Systems Technology, IEEE Transactions on*, 11(6):839–849, 2003.

[8] Yi L. Murphey, ZhiHang Chen, Leonidas Kiliaris, and M. Abul Masrur. Intelligent power management in a vehicular system with multiple power sources. *Journal of Power Sources*, 196(2):835 – 846, 2011.

[9] Yasha Parvini, Ernesto G. Urdaneta, Jason B Siegel, Saemin Choi, Ardalan Vahidi, and Levi Thompson. Range extension study of a hybridized lead-acid battery using ultracapacitors via simulation and experimental results from a 12 volt actively controlled hardware in the loop test bench. 2014. in preparation.

[10] P Rodatz, G Paganelli, A Sciarretta, and L Guzzella. Optimal power management of an experimental fuel cell/supercapacitor-powered hybrid vehicle. *Control Engineering Practice*, 13(1):41–53, 2005.

[11] Alexander N Wilhelm, Brian W Surgenor, and Jon G Pharoah. Design and evaluation of a micro-fuel-cell-based power system for a mobile robot. *Mechatronics, IEEE/ASME Transactions on*, 11(4):471–476, 2006.